Atmos. Meas. Tech., 8, 3433–3445, 2015
www.atmos-meas-tech.net/8/3433/2015/
doi:10.5194/amt-8-3433-2015
© Author(s) 2015. CC Attribution 3.0 License.

Atmospheric Measurement Techniques
Open Access

Quantifying lower tropospheric methane concentrations using GOSAT near-IR and TES thermal IR measurements

J. R. Worden[1], A. J. Turner[2], A. Bloom[1], S. S. Kulawik[3], J. Liu[1], M. Lee[1], R. Weidner[1], K. Bowman[1], C. Frankenberg[1], R. Parker[4], and V. H. Payne[1]

[1]Earth Sciences Section, Jet Propulsion Laboratory/CalTech, Pasadena, USA
[2]School of Engineering and Applied Sciences, Harvard University, Cambridge, MA, USA
[3]Bay Area Environmental Research Institute, Mountain View, CA, USA
[4]Dept. of Physics and Astronomy, University of Leicester, Leicester, UK

Correspondence to: J. R. Worden (john.worden@jpl.nasa.gov)

Received: 29 March 2015 – Published in Atmos. Meas. Tech. Discuss.: 20 April 2015
Revised: 22 July 2015 – Accepted: 13 August 2015 – Published: 25 August 2015

Abstract. Evaluating surface fluxes of CH_4 using total column data requires models to accurately account for the transport and chemistry of methane in the free troposphere and stratosphere, thus reducing sensitivity to the underlying fluxes. Vertical profiles of methane have increased sensitivity to surface fluxes because lower tropospheric methane is more sensitive to surface fluxes than a total column, and quantifying free-tropospheric CH_4 concentrations helps to evaluate the impact of transport and chemistry uncertainties on estimated surface fluxes. Here we demonstrate the potential for estimating lower tropospheric CH_4 concentrations through the combination of free-tropospheric methane measurements from the Aura Tropospheric Emission Spectrometer (TES) and XCH_4 (dry-mole air fraction of methane) from the Greenhouse gases Observing SATellite – Thermal And Near-infrared for carbon Observation (GOSAT TANSO, herein GOSAT for brevity). The calculated precision of these estimates ranges from 10 to 30 ppb for a monthly average on a $4° \times 5°$ latitude/longitude grid making these data suitable for evaluating lower-tropospheric methane concentrations. Smoothing error is approximately 10 ppb or less. Comparisons between these data and the GEOS-Chem model demonstrate that these lower-tropospheric CH_4 estimates can resolve enhanced concentrations over flux regions that are challenging to resolve with total column measurements. We also use the GEOS-Chem model and surface measurements in background regions across a range of latitudes to determine that these lower-tropospheric estimates are biased low by approximately 65 ppb, with an accuracy of approximately 6 ppb (after removal of the bias) and an actual precision of approximately 30 ppb. This 6 ppb accuracy is consistent with the accuracy of TES and GOSAT methane retrievals.

1 Introduction

Advances in remote sensing in the last decade have resulted in global mapping of atmospheric methane concentrations (e.g., Frankenberg et al., 2005, 2011; Worden et al., 2012) that in turn have provided new insights into the role of wetlands (e.g., Bloom et al., 2010), fires (e.g., Worden et al., 2012, 2013), the stratosphere (e.g., Xiong et al., 2013), and anthropogenic emissions (e.g. Kort et al., 2014) on tropospheric methane concentrations. However, use of these data to improve global flux estimates and their trends of either methane or CO_2, relative to measurements from the surface network, is challenging in part because of their measurement accuracy and sampling (e.g., Bergamaschi et al., 2013) or because these measurements are primarily sensitive to methane over the whole column or the free troposphere and stratosphere, which have long mixing length scales (e.g., Keppel-Aleks et al., 2011, 2012; Wecht et al., 2012; Worden et al., 2013). For example, Fig. 1 shows a methane profile derived from Aura Tropospheric Emission Spectrometer (TES) radiances during July 2009. Because the amount of methane within a sub-column of the profile scales approximately with the pressure difference of the layer boundaries, less than 25 % of the total column is typically in the boundary

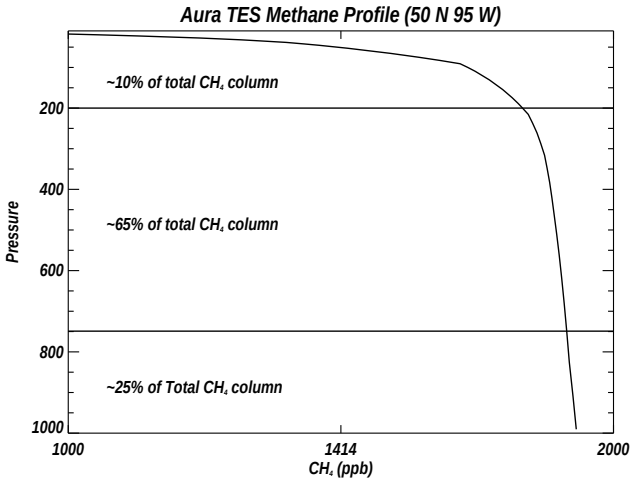

Figure 1. A retrieved methane profile from the Aura TES instrument during July 2009.

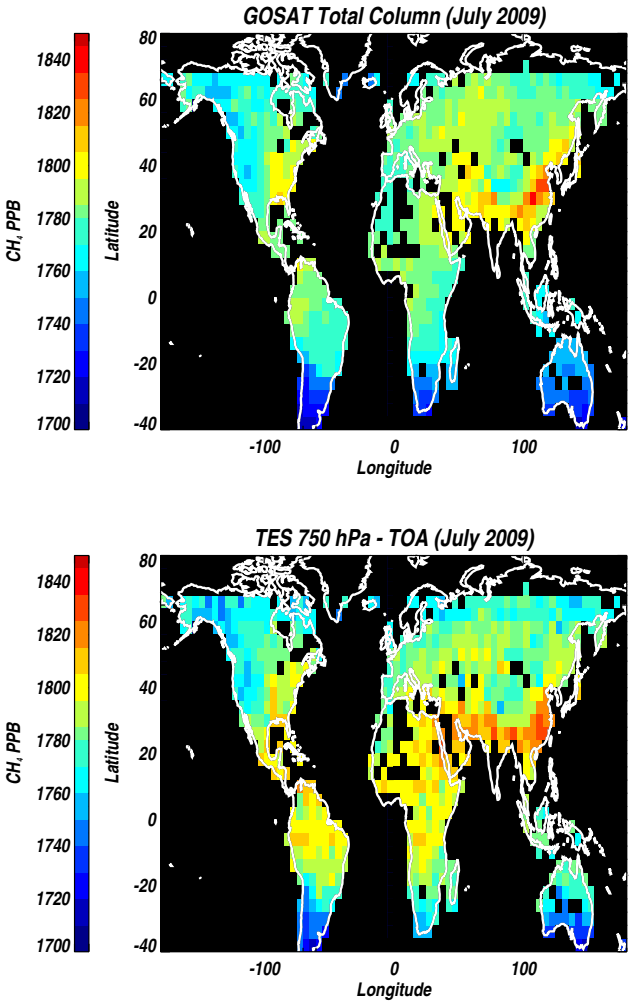

Figure 2. Top: XCH_4 from the GOSAT instrument. Black indicates no data. Bottom: XCH_4 from the Aura TES instrument for the free troposphere to stratosphere (typically 750 hPa to TOA). Black indicates no data.

layer where it is most sensitive to the underlying surface fluxes with the remaining column amount in the free troposphere or stratosphere. Figure 2 shows averaged total column measurements derived from GOSAT radiance measurements (e.g., Parker et al., 2011, and references therein) and free-tropospheric measurements from the Aura TES instrument (Worden et al., 2012) for July 2009 (see Appendix B and Sect. 2.3). Although the total column measurements are more sensitive to near-surface measurements than the TES measurements, both measurements broadly see similar features because they are both strongly sensitive to the bulk of the methane column. The largest methane values occur over the eastern parts of North America and Asia and moderate values of CH_4 over central Asia. Lowest values of the total column are at high-latitudes because the fractional contribution of the depleted stratosphere to the total column becomes larger with increasing latitude for both data sets. Uncertainties in both of these measurements also increase with latitude because the signal-to-noise ratio of total-column measurements depends on reflected sunlight and the signal-to-noise ratio of thermal infrared based measurements depends on temperature, both of which decrease with increasing latitude. Atmospheric methane concentrations above the lower troposphere are primarily sensitive to fluxes that are hundreds to thousands of kilometers away, depending on the latitude (e.g., Keppel-Aleks et al., 2011, 2012; Worden et al., 2013). Therefore, uncertainties in transport, both vertical and horizontal, are important to consider when using these data to investigate underlying fluxes or processes (e.g., Stephens et al., 2007; Jiang et al., 2013, 2015; Worden et al., 2013).

We next examine the sensitivity of a total column and lower troposphere column to changes in the underlying fluxes. Figure 3 shows methane fluxes used in Version 9.0.2 of the GEOS-Chem global chemical transport model (see Appendix A as well as Bey et al., 2001; Kaplan, 2002; Pickett-Heaps et al., 2011; Wecht et al., 2012, 2014; Turner et al., 2015). Fluxes above 50° N are primarily due to wetlands whereas those at lower latitudes are primarily due to a combination of fossil fuels, wetlands, rice farming, and agriculture. Figure 4 (top panel) shows a comparison between modeled XCH_4 above the Hudson Bay lowlands ($\sim$ 52° N, 85° W) to XCH_4 if the modeled southern Hudson Bay lowland (HBL) wetland fluxes between 48 to 66° N and 100 to 70° W are reduced by half. The total column differences in the summer between these two model runs are approximately 10 ppb, about the same as the precision of a single total column measurement from the GOSAT TANSO (Greenhouse gases Observing SATellite – Thermal And Near-infrared for carbon Observation) satellite (Sect. 2). Consequently, substantial averaging and sampling is required to quantify these high-latitude fluxes even to within a factor of two using total column data. In contrast, Fig. 4 (bottom panel) shows

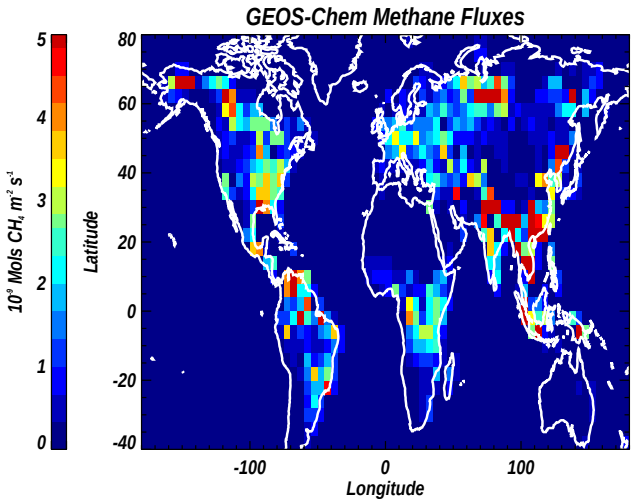

Figure 3. Methane fluxes used in GEOS-Chem model.

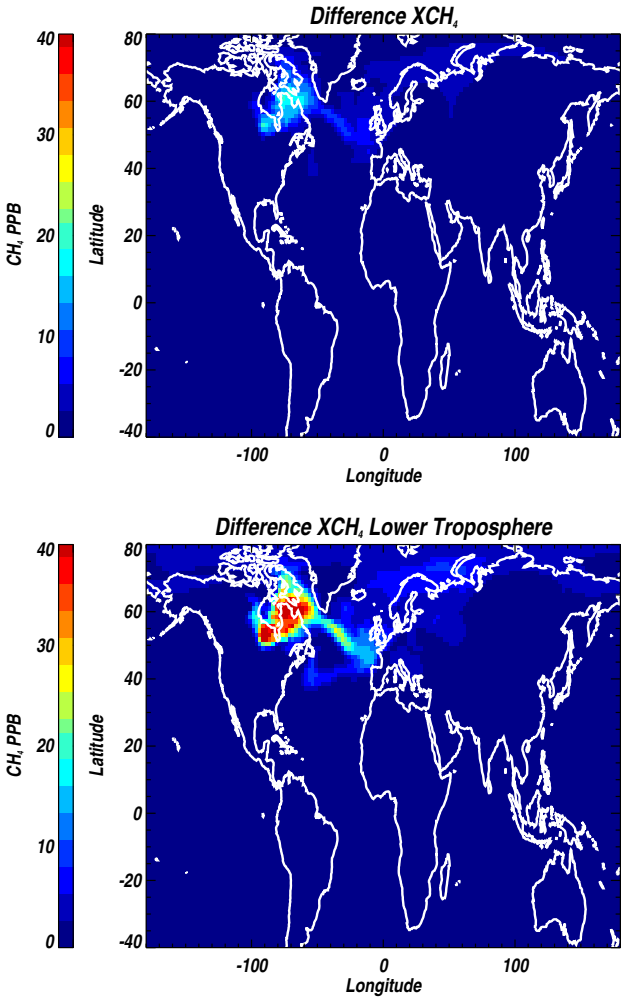

Figure 4. Top: difference in XCH_4 between a reference GEOS-Chem run and another in which the Hudson Bay lowland flux (48 to 66° N and 100 to 70° W) has been reduced by half. Bottom: same as in top panel but for the lower troposphere.

the effect of this perturbation is much stronger in the lowermost troposphere (the lowermost 250 hPa of atmosphere or approximately surface to 750 hPa) with differences of approximately 40 ppb near the source region. Increasing the sensitivity of remote sensing measurements to the underlying surface fluxes is therefore our motivation for this study. We therefore evaluate the capability of estimating lower tropospheric methane concentrations using GOSAT short-wave infrared (SWIR) and TES thermal infrared (TIR) measurements because the combination of these measurements provides greater sensitivity to the underlying fluxes and reduced sensitivity to transport error (e.g., Jiang et al., 2015, and references therein) than either the SWIR or the TIR based measurements alone.

We next present a comparison between GOSAT and TES data. We then derive the instrument operator for lower tropospheric estimates based on the GOSAT/TES data. We compare these data to lower-tropospheric concentrations from GEOS-Chem in order to help assess the calculated sensitivity and sampling errors. We then calculate a total error budget for these estimates followed by a comparison to surface data.

2 Estimating lower-tropospheric methane from GOSAT and TES

Recent advances in remote sensing show that combining reflected sunlight and thermal IR measurements to estimate trace gas profiles can provide improved vertical resolution compared to measurements from either individual wavelength region (e.g., Worden et al., 2007; H. M. Worden et al., 2010; Kuai et al., 2013). In the case where the trace gas varies significantly in the free troposphere, it is necessary to estimate the trace gas profile from the radiances when the reflected sunlight and thermal IR measurement observe the same air parcel (e.g., H. M. Worden et al., 2010). For long-lived trace gases such as CO_2 (e.g., Kuai et al., 2013) we can subtract the free-tropospheric/stratospheric posterior estimate (based on thermal IR radiances) from the total column (based on reflected sunlight radiances). In this case observations that are not exactly co-located in space and time can be used together to estimate lower-tropospheric concentrations because of the long mixing length scales of these trace gases in the free troposphere and stratosphere (Sect. 3). We therefore use the approach described in Kuai et al. (2013) for estimating lower tropospheric CH_4 measurements in which the thermal IR measurement from TES, which provides information about atmospheric methane concentrations from approximately 750 hPa through the stratosphere is subtracted from the total column estimates from the GOSAT measurement. For example, Fig. 5 shows an example of the sensitivity of the total column average volume mixing ratio (VMR) of methane from the GOSAT and TES and retrievals (see Appendix B

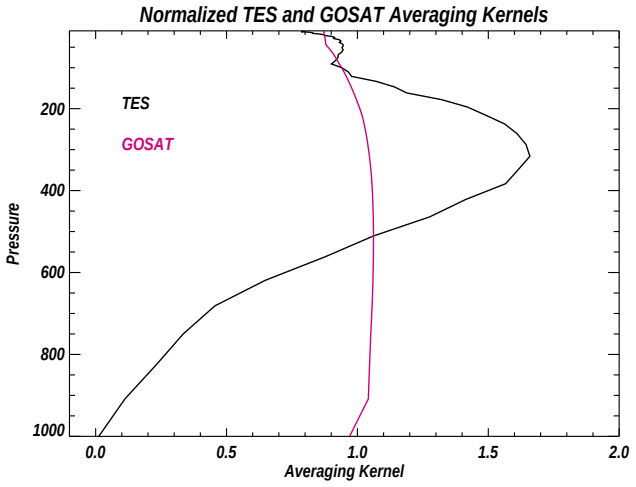

Figure 5. Sensitivity (or averaging kernel) of the total column with respect to the retrieved GOSAT and TES methane profile. Both averaging kernels have been normalized by the sub-column of each layer in the profile.

for a summary of the GOSAT and TES retrieval characteristics and data source) respectively to the methane profile (in terms volume mixing ratio or VMR). Both averaging kernels are normalized by the column of each sub-layer (e.g., Eq. 8 in Connor et al., 2008, or O'Dell et al., 2012); the GOSAT retrievals are approximately uniformly sensitive to methane at all levels whereas the TES retrievals have peak sensitivity in the middle/upper troposphere and declining sensitivity towards the surface.

2.1 Estimation approach

The retrieved column amount is a function of the prior information, sensitivity, the true state, and uncertainties:

$$\hat{C} = C^{\mathrm{a}} + C_{\mathrm{air}}\boldsymbol{h}^{\mathrm{T}}\mathbf{A}(\boldsymbol{x} - \boldsymbol{x}^{\mathrm{a}}) + \Sigma_i C_i \boldsymbol{h}^{\mathrm{T}}\boldsymbol{\delta}_i. \quad (1)$$

We define Eq. (1) such that $\hat{C}$ is the estimated total column in units of molecules cm^{-2} so that we can conveniently subtract the TES free-tropospheric and stratospheric column amount from the total column amount measured by GOSAT. The $\boldsymbol{h}$ is the column operator that relates trace gases given in volume mixing ratio (VMR) to the average column mixing ratio (typically given in the literature as X_{CH4} for methane), the C_{air} variable is the total dry air column and converts the average column mixing ratio into the dry air column in units of molecules cm^{-2}, the $\mathbf{A}$ is the averaging kernel matrix or $\mathbf{A} = \frac{\partial \hat{\boldsymbol{x}}}{\partial \boldsymbol{x}}$, where $\boldsymbol{x}$ is the true state and $\hat{\boldsymbol{x}}$ is the estimate of the true state (e.g., Rodgers, 2000). The superscript "a" refers to the a priori used to constrain the retrieval. The summation over $\boldsymbol{\delta}$ refers to all the errors included with this estimate, mapped to a column amount using the $\boldsymbol{h}$ operator (see Appendix B for summary of the errors in TES and GOSAT data). Note that the TES data are reported on a log VMR grid. The GOSAT averaging kernels are already mapped to a pressure-weighted column relative to $\boldsymbol{x}$, which is a one-dimensional vector that is linear in VMR. Both sets of averaging kernels must be converted to the same units prior to comparison.

The GOSAT averaging kernels have been pre-mapped into a "column" averaging kernel, $a = (\boldsymbol{h}^{\mathrm{T}}\mathbf{A})_j/\boldsymbol{h}_j$, (e.g., Connor et al., 2008) where the subscript j refers to the pressure levels of the GOSAT retrieval grid. The TES averaging kernels are reported on the forward model pressure levels used in the TES radiative transfer algorithm. For the next set of equations we find it useful to use the nomenclature $\boldsymbol{b} = \boldsymbol{h}^{\mathrm{T}}\mathbf{A}$ which can be computed from the GOSAT averaging kernels. We next divide up the columns into a lower-tropospheric component (consisting of the pressure levels for the lowermost 250 hPa of the atmosphere or typically surface to 750 hPa), and the rest of the atmosphere. The column amount for the lowermost troposphere can then be given as

$$\hat{C}_{\mathrm{L}} = \hat{C}_{\mathrm{tot}} - \hat{C}_{\mathrm{U}}, \quad (2)$$

where we will use GOSAT to provide the total column and TES to provide the upper tropospheric column (denoted by subscripts "tot" and "U" respectively).

Using Eq. (1) we can re-write Eq. (2) as

$$\hat{C}_{\mathrm{L}} = C^{\mathrm{a}}_{\mathrm{L}} + C_{\mathrm{air}}\boldsymbol{b}^{\mathrm{G}}_{\mathrm{L}}(\boldsymbol{x}_{\mathrm{L}} - \boldsymbol{x}^{\mathrm{a}}_{\mathrm{L}}) + C^{\mathrm{a}}_{\mathrm{U}} + C_{\mathrm{air}}\boldsymbol{b}^{\mathrm{G}}_{\mathrm{U}}(\boldsymbol{x}_{\mathrm{U}} - \boldsymbol{x}^{\mathrm{a}}_{\mathrm{U}}) - \quad (3a)$$

$$(C^{\mathrm{a}}_{\mathrm{U}} + C^{\mathrm{air}}_{\mathrm{U}}\boldsymbol{h}^{\mathrm{T}}_{\mathrm{U}}\mathbf{A}^{\mathrm{TES}}_{\mathrm{UU}}(\boldsymbol{x}_{\mathrm{U}} - \boldsymbol{x}^{\mathrm{a}}_{\mathrm{U}}) + C^{\mathrm{air}}_{\mathrm{U}}\boldsymbol{h}^{\mathrm{T}}_{\mathrm{U}}(\mathbf{A}^{\mathrm{TES}}_{\mathrm{UL}})(\boldsymbol{x}_{\mathrm{L}} - \boldsymbol{x}^{\mathrm{a}}_{\mathrm{L}}))$$
$$+ \Sigma_i C_i \boldsymbol{h}^{\mathrm{T}}\boldsymbol{\delta}_i. \quad (3b)$$

Equation (3a) represents the GOSAT contribution to the total tropospheric column amount estimate in Eqs. (2) and (3b) represents the TES contribution to the upper tropospheric column. The subscript "L" refers to the pressure levels that make up the "lower troposphere", the subscript "U" refers to the pressure levels that make up the free troposphere and stratosphere, the superscript "G" refers now to the GOSAT averaging kernel and the superscript "TES" refers to the TES averaging kernel. The subscripts "UU" and "LL" indicate the block diagonal part of the averaging kernel matrix ($\mathbf{A}$) corresponding to the "U" and "L" levels, respectively. Because $\boldsymbol{b} = \boldsymbol{h}^{\mathrm{T}}\mathbf{A}$, the vector $\boldsymbol{b}_{\mathrm{U}}$ refers to the "u" set of pressure levels for the vector $\boldsymbol{b}$ and is not the same as $\boldsymbol{h}_{\mathrm{U}}\mathbf{A}_{\mathrm{UU}}$. Note that we have assumed for the sake of simplicity that the a priori constraint vectors (e.g., $\boldsymbol{x}_{\mathrm{a}}$) are the same for the GOSAT and TES retrievals as we can always swap one prior with another (e.g., Rodgers and Connor, 2003). The second part of Eq. (3b) also includes the cross term "UL" which describes the impact on the upper-tropospheric methane from the lower tropospheric estimate of methane in the TES retrieval (e.g., Worden et al., 2004). We drop this term in subsequent equations as we find it is much smaller than the other terms. The last term in Eq. (3b) describes the various uncertainties affecting the GOSAT and TES retrievals.

Equation (3) can be re-written as

$$\hat{C}_{\mathrm{L}} = C_{\mathrm{L}}^{\mathrm{a}} + C_{\mathrm{air}} \boldsymbol{b}_{\mathrm{L}}^{\mathrm{G}} \left(\boldsymbol{x}_{\mathrm{L}} - \boldsymbol{x}_{\mathrm{L}}^{\mathrm{a}}\right) + C_{\mathrm{air}} \left(\boldsymbol{b}_{\mathrm{U}}^{\mathrm{G}} - \propto \boldsymbol{h}_{\mathrm{U}}^{\mathrm{T}} \mathbf{A}_{\mathrm{UU}}^{\mathrm{TES}}\right) \left(\boldsymbol{x}_{\mathrm{U}} - \boldsymbol{x}_{\mathrm{U}}^{\mathrm{a}}\right) + \sum\nolimits_i C_i \boldsymbol{h}^{\mathrm{T}} \boldsymbol{\delta}_i, \quad (4)$$

where $\propto = C_{\mathrm{U}}^{\mathrm{air}} / C_{\mathrm{air}}$ and the variable C_i in the right side of Eq. (4) refers to either the total column or the upper tropospheric column, depending on the vertical range of the corresponding error. Typically, data assimilation or inverse estimates of fluxes involve applying the averaging kernel from the data to the model, which includes the averaging kernel terms in Eq. (3a) and (3b). For the comparison discussed in this paper, we will apply Eq. (2) (equivalent to Eq. 4, but without uncertainties in the last term of Eq. 4) to the GEOS-Chem model fields. Because the TES and GOSAT instruments do not typically observe the same air parcel, we also must use the approach of subtracting a monthly average of the free-tropospheric CH_4 column (based on TES) from the monthly averaged total column based on GOSAT data. This approach will incur a "co-location" error that we evaluate in Sect. 3.2 using the GEOS-Chem model and the TES and GOSAT averaging kernels. A more sophisticated approach using both data sets could be to assimilate the TES CH_4 fields in order to minimize errors in the model transport and chemistry and then use the GOSAT data to estimate model fluxes (e.g., Kuai et al., 2013). This approach is potentially the subject of a future investigation, but is beyond the scope of this current investigation because of the complexities of the data assimilation framework.

2.2 Lower-tropospheric estimates and comparison to GEOS-Chem

We choose to estimate data for July 2009 because (1) both TES and GOSAT have the best overall sampling during this time period and (2) we want to evaluate how sensitive these lower-tropospheric estimates are to high-latitude fluxes. Figure 6 (top panel) shows the July 2009 monthly estimate of XCH_4 for the lower troposphere (lowermost 250 hPa of the atmosphere) and Fig. 6 (bottom panel) shows the corresponding GEOS-Chem model values after applying the TES and GOSAT averaging kernels, sampling, monthly averaging and subtraction used for the TES and GOSAT lower tropospheric estimate. A global bias of approximately 65 ppb is added to the GOSAT/TES lower tropospheric values (see Sect. 3.5). The largest near-surface concentrations are in the northern latitudes, as expected by the model (Fig. 6), and are a result of summertime fluxes of wetlands (e.g., Fig. 3). A combination of biogenic and anthropogenic emissions are responsible for the larger concentrations on the eastern coasts of North America and Asia with tropical enhancements of methane associated with the source regions in the western Amazon and Congo regions.

Figure 7 (top panel) shows the difference between the estimated lower-tropospheric methane with respect to the

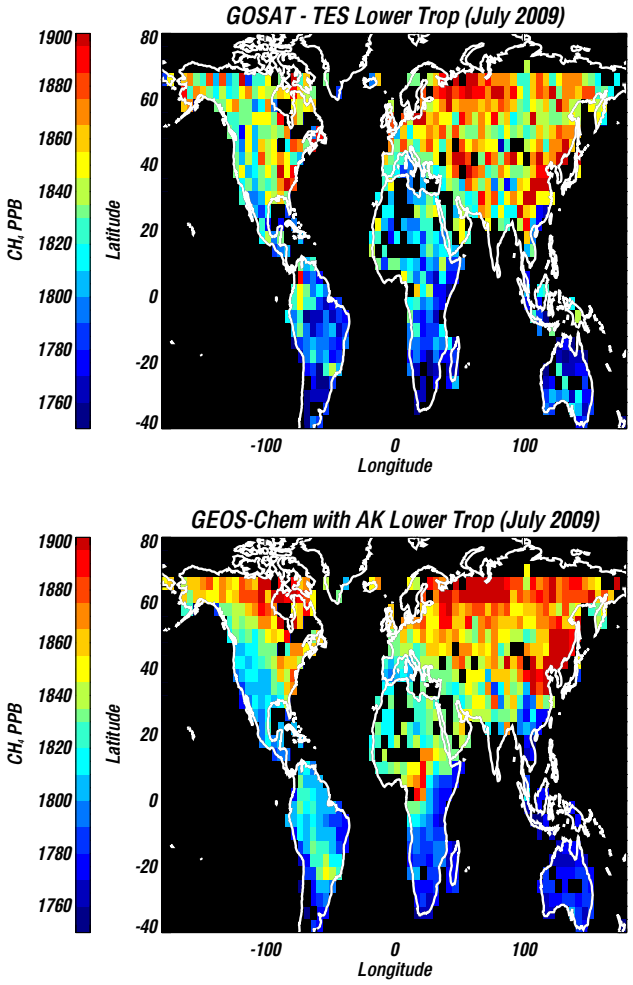

Figure 6. Top: CH_4 lower-tropospheric estimate using GOSAT and TES data. Black indicates no data. Bottom: lower-tropospheric estimate from GEOS-Chem model for the same latitudes and longitudes shown in top panel of Fig. 6.

corresponding GEOS-Chem values. As discussed in subsequent sections, the precision of these data ranges from 10 to 30 ppb with an accuracy of approximately 6 ppb (after a global bias correction). Consequently regions that are higher than 50 ppb or more (red color) or lower than −50 ppb or less (blue colors) are regions where the modeled fluxes are likely in significant disagreement with the true fluxes. The largest data/model differences are typically over flux regions (Fig. 3) and suggest that the high-latitude wetland fluxes are too large in the GEOS-Chem model and too low in Europe, North America, and Asia. A large region between the Black and Caspian seas ($\sim 40^\circ$ N, 40° E) is also under-represented in the model. For comparison, Fig. 7 (bottom panel) shows the total column differences between GOSAT and GEOS-Chem after a global mean bias of ~ -9.5 ppb is removed. As with Fig. 4, the comparison between the top and bottom panels of Fig. 7 empirically demonstrates the increased

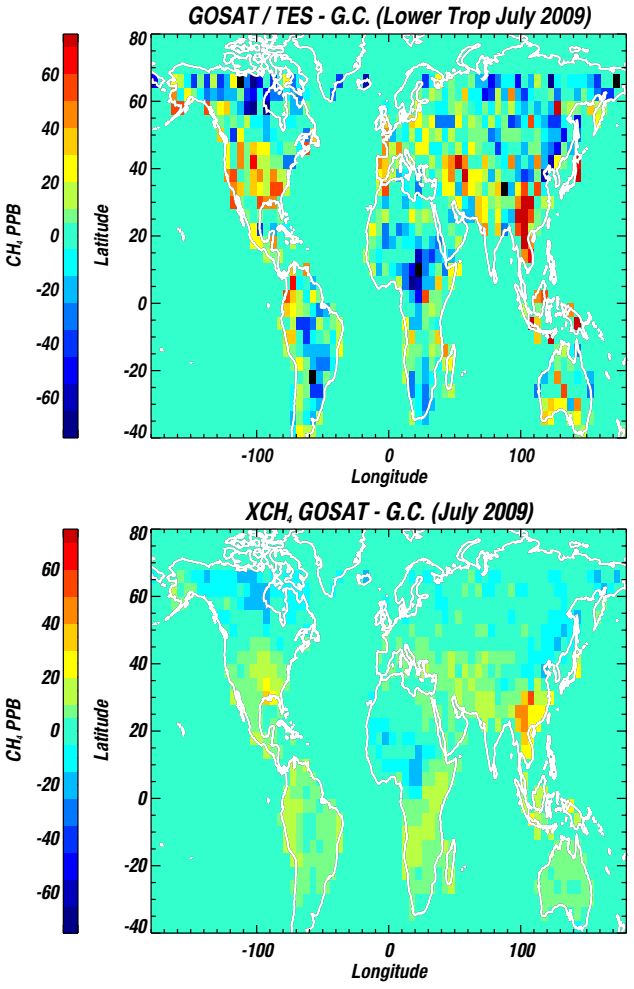

Figure 7. Top: difference in lower-tropospheric estimate between GOSAT/TES and the GEOS-Chem model. Black indicates no data. Bottom: difference in total column estimate between GOSAT and the GEOS-Chem model.

sensitivity of the lower-tropospheric methane to the underlying methane fluxes as there are significantly larger variations in the lower-tropospheric methane estimates over the larger flux regions. This comparison also shows how use of the total column alone can lead to erroneous conclusions as the total column data is biased high with respect to the model over South America but the lower-tropospheric estimate comparison shows much more significant variation, with a positive bias in northern Amazonia and a negative bias in middle Amazonia and Southern Brazil. In addition, the data/model difference for the total column shows very little variation over the Siberian and northern European wetlands indicating little sensitivity to this important component of the global methane budget.

3 Error analysis

We can calculate the "error" statistics of the lower tropospheric methane estimates by subtracting the "true" lower tropospheric column amount ($\boldsymbol{h}_{\mathrm{L}}^{\mathrm{T}}\boldsymbol{x}_{\mathrm{L}}$) from Eq. (4) and computing the expectation of this difference:

$$||(\hat{C}_{\mathrm{L}} - C_{\mathrm{L}})(\hat{C}_{\mathrm{L}} - C_{\mathrm{L}})^{\mathrm{T}}|| = C_{\mathrm{air}}^2(\boldsymbol{b}_{\mathrm{L}}^{\mathrm{G}} - \boldsymbol{h}_{\mathrm{L}}^{\mathrm{T}})\mathbf{S}_{\mathrm{LL}}(\boldsymbol{b}_{\mathrm{L}}^{\mathrm{G}} - \boldsymbol{h}_{\mathrm{L}}^{\mathrm{T}})^{\mathrm{T}}$$
$$+ C_{\mathrm{air}}^2(\boldsymbol{b}_{\mathrm{U}}^{\mathrm{G}} - \propto \boldsymbol{h}_{\mathrm{U}}^{\mathrm{T}}\mathbf{A}_{\mathrm{UU}}^{\mathrm{TES}})\mathbf{S}_{\mathrm{UU}}(\boldsymbol{b}_{\mathrm{U}}^{\mathrm{G}} - \propto \boldsymbol{h}_{\mathrm{U}}^{\mathrm{T}}\mathbf{A}_{\mathrm{UU}}^{\mathrm{TES}})^{\mathrm{T}}$$
$$+ \Sigma_i C_i^2 \boldsymbol{h}^{\mathrm{T}}\mathbf{S}_i\boldsymbol{h}, \quad (5)$$

where the C_{L} is the "true" lower tropospheric column amount and the $\mathbf{S}_i$ term describes the statistics (or error covariance) of the error terms δ in Eq. (3). The first two terms on the right-hand side effectively describes the "smoothing error" (Rodgers, 2000) for the lower-tropospheric estimate. A comparison between model (e.g., GEOS-Chem) and data (e.g. GOSAT minus TES) does not need to compare against this smoothing error term as it is removed if the GOSAT and TES averaging kernels are first applied to the model fields. However, we will estimate the smoothing error in the next section (Sect. 3.1) for completeness. Note that there is also a cross term in this expression that we have ignored because it depends on the atmospheric methane correlations between the upper troposphere and lower troposphere, which are small, and the term $\boldsymbol{b}_{\mathrm{L}} - \boldsymbol{h}_{\mathrm{L}}$, which is also small as discussed in next section.

Uncertainties due to noise and radiative interferences will need to be calculated for any model/data comparison. These errors are contained in the TES and GOSAT product files as discussed in Worden et al. (2012), Parker et al. (2011) and references therein. The error on the lower-tropospheric column amount will have a much larger percentage error than the total and free-tropospheric estimates for XCH_4 because Eq. (2) subtracts two large numbers with similar percentage uncertainties to obtain a smaller number. However, for this comparison we average a month's worth of data over a $4^\circ \times 5^\circ$ lat/lon grid box, which reduces the random component of this error (e.g., Kuai et al., 2013).

We also need to calculate two additional error sources from the following: (1) the assumption that we can average GOSAT and TES posterior columns on a chosen grid box (in this case $4^\circ \times 5^\circ$) even though the GOSAT and TES observations are not necessarily co-located and (2) knowledge error of the XCO_2 distribution used to estimate XCH_4 concentrations from the GOSAT CH_4/CO_2 "proxy" retrieval.

3.1 Smoothing error from the free-troposphere column

The "smoothing error" (Rodgers, 2000) for the lower-tropospheric estimate is given by the first two terms on the right-hand side of Eq. (5). This term is composed of the smoothing error corresponding to the lower-tropospheric levels and the cross state error, which is the impact of the upper-tropospheric estimate on the lower-tropospheric estimate.

Both of these errors are removed from any model profile/data comparison if the model is first adjusted with the TES and GOSAT averaging kernels and a priori constraints (or the instrument operators) prior to comparison. However, if only the lower-tropospheric component is compared to the model, in order to mitigate model transport and chemistry errors in a data/model comparison, then the second term needs to be included in the overall error budget. We find that the first component of the smoothing error (first term of Eq. 5) is negligible because the expression $\boldsymbol{b}_{\mathrm{L}} - \boldsymbol{h}_{\mathrm{L}}$ is almost identical to zero. In fact, this term is approximately 1 ppb even for assumed covariances of up to 200 ppb (squared) in the lower troposphere. We can evaluate the second term (or cross-state error) error an a priori methane climatology from the GEOS-Chem model and the averaging kernels from TES and GOSAT and in general find it to be less than 15 ppb. Note that the TES and GOSAT averaging kernels must both be mapped to the same units and dimensions.

3.2 Co-location error

As discussed previously, most TES and GOSAT observations do not observe the same air parcel; consequently, in order to estimate lower-tropospheric CH_4 abundances we subtract monthly averaged free-tropospheric/stratospheric columns (or typically 750 to TOA), derived from the TES CH_4 profile estimates, from monthly averages of the GOSAT total column:

$$\hat{C}_{\mathrm{L}}^{\mathrm{M}} = \hat{C}_{\mathrm{TOT}}^{\mathrm{M}} - \hat{C}_{\mathrm{U}}^{\mathrm{M}}, \tag{6}$$

where the superscript "M" refers to the monthly average. An error results from this assumption because the 750 to TOA column changes over a month due to transport. For model profile/data comparisons using Eqs. (2) or (5), this error is not included in the total error budget because the model is typically sampled at the observations' spatiotemporal coordinates. However, this error will need to be considered for comparison to monthly averages of aircraft data, for example.

We evaluate this uncertainty by using the GEOS-Chem model and the TES averaging kernels. We first calculate the free-tropospheric CH_4 column (750 hPa to TOA) by applying Eq. (3) to the GEOS-Chem model and using the TES spatiotemporal sampling. We then perform the same operation but with the GOSAT spatiotemporal sampling and the nearest TES averaging kernels to these spatiotemporal coordinates. We find that the mean RMS (Root Mean Square) difference in the monthly averaged $4^\circ \times 5^\circ$ binned free-tropospheric sub-column is approximately 7 ppb or less and is effectively random as a function of latitude. We add this uncertainty into the total error budget by computing the RMS of the difference as a function of latitude (Sect. 3.4).

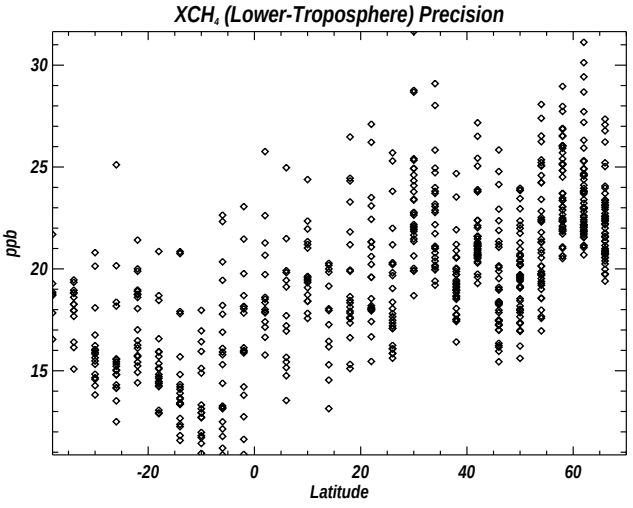

Figure 8. Estimated total precision for the GOSAT/TES lower tropospheric CH_4 estimates.

3.3 Total precision

The precision of these estimates can be calculated from the sum of the observation error covariances (noise and spectral interferences), the co-location error, and cross-state error. The observation covariances for a monthly average in each grid box are effectively reduced relative to a single measurement by the square root of the number of observations. Figure 8 shows the precision as a function of latitude. The precision varies from 10 to 30 ppb and generally varies with latitude likely because the observation error and sampling becomes poorer for both TES and GOSAT at higher latitudes. However, this precision is sufficient to resolve, for example, the high-latitude lower-tropospheric concentrations over the Siberian wetlands from the adjacent Russian boreal forest as well as the Canadian wetlands. We next compare these data to surface measurements to evaluate the actual precision and to estimate the accuracy.

3.4 Comparison to surface data and estimate of accuracy

Direct comparison of these lower tropospheric estimates to surface data must account for variability in surface methane as well as methane in the boundary layer and residual component of the free troposphere that makes up the lower tropospheric column. For this reason we use the GEOS-Chem model shown in Fig. 6 as a way of comparing the GOSAT/TES data to surface sites. We compare to surface sites available from the World Data Centre for Greenhouse Gases (WDCGC: http://ds.data.jma.go.jp/gmd/wdcgg/). These data are typically in background regions which will mitigate uncertainties in data/model comparisons because of large possible differences between the fluxes used in GEOS-Chem and the actual fluxes as demonstrated by the

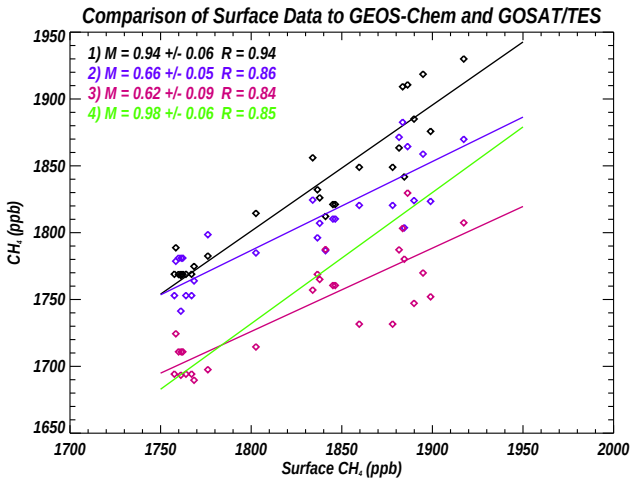

Figure 9. (1: Black) Comparison of GEOS-Chem surface values to monthly surface methane (averaged) measurements from the WDCGC. (2: Blue) GEOS-Chem lower-tropospheric methane vs. surface measurements. (3: Red) GOSAT/TES lower tropospheric methane vs. surface measurements. (4: Green) GOSAT/TES lower tropospheric methane based on CMS XCO_2 values vs. surface methane measurements. The diamonds are the different data sets and the lines are linear fits to the data. The variable M is the slope of the fitted line and the variable R is the correlation coefficient.

near surface concentration differences shown in the top panel of Fig. 7. Only sites in continental regions are used because of sparse sampling by the GOSAT instrument over island sites. Based on these criteria there are 27 sites available from the WDCGC network that can be compared to these lower-tropospheric data (Appendix C).

Figure 9 shows a least squares fit between monthly averaged surface measurements and monthly averaged GEOS-Chem surface values for the sites discussed in Appendix C (black diamonds). The least squares fit assumes an uncertainty of 11 ppb for the GEOS-Chem model based on the scatter in the data. For many sites, only monthly values are provided, and therefore we assume in an ad hoc manner that the error on the mean for these monthly values are also 11 ppb. Using these estimates we find that the GEOS-Chem surface methane concentrations have effectively the same variability as the surface sites with a slope of 0.94 ± 0.06 and a correlation of 0.94. The mean difference between GEOS-Chem surface methane and the surface methane data is 0.46 ppb with an RMS of 20.3 ppb corresponding to an error on the mean difference of approximately 4 ppb.

The blue diamonds (and corresponding line) in Fig. 9 show a comparison between the lower-tropospheric estimates in GEOS-Chem, corresponding to those from the GOSAT/TES measurements, and the surface data. This comparison also demonstrates how methane variability in the lower troposphere is less than on the surface. The red diamonds are a least squares fit between the surface data and the GOSAT/TES data.

The RMS difference between the GEOS-Chem and the GOSAT/TES data for these sites is approximately 22 ppb. The sum (in quadrature) of the RMS differences between GEOS-Chem and the surface and GEOS-Chem and GOSAT/TES data is approximately 30 ppb, which is consistent but slightly larger than the precision shown in Fig. 8. The mean difference between the GOSAT/TES data and the GEOS-Chem data is approximately 65 ± 4.4 ppb and the mean difference between the GEOS-Chem surface methane and the surface sites is 0.4 ± 3.7 ppb. Including the error on the mean between the GEOS-Chem model and surface data, the bias in the GOSAT/TES data is approximately 65 ± 6 ppb. We therefore estimate that the accuracy is approximately 6 ppb for these measurements after the bias of 65 ppb is removed. This result is consistent in sign but not quite the magnitude with the positive bias in TES that is approximately 28 ± 5 ppb (Alvarado et al., 2015; note that the Alvarado et al., 2015, paper computes the RMS of TES minus aircraft data which is about 30 ppb, whereas the error on the mean is the error of the bias and is approximately 5 ppb) and the negative bias in GOSAT that is approximately -17 ± 0.2 ppb for the GOSAT proxy retrievals (e.g. Schepers et al., 2012).

3.5 CO_2 bias error

As discussed in Frankenberg et al. (2011), Butz et al. (2010), and Parker et al. (2011) the XCH_4 estimates used in this study are derived using the following approach. First XCH_4 and XCO_2 are estimated from radiances in the 1.6 micron band. Then, the XCH_4 value is divided by the XCO_2 value in order to mitigate effects from interferences such as from aerosols and surface albedo. The assumption here is that the XCO_2 and XCH_4 values derived from the 1.6 micron radiances are affected in a nearly identical manner by the interferences in this band. Finally, this ratio is multiplied by XCO_2 derived from the Carbontracker model (Peters et al., 2007). A potential source of uncertainty in the XCH_4 estimate and consequently these lower tropospheric estimates is from variable bias error in the total CO_2 column from Carbontracker used to infer the CH_4 column. For example, a bias error of 1 % in XCO_2 directly leads to a 4 % bias error in the lower-tropospheric sub-column between 1000 and 750 hPa, or approximately 80 ppb for CH_4 in the lower troposphere. We test the effects of XCO_2 knowledge error on our estimates of lower-tropospheric CH_4 concentrations by first re-normalizing the XCH_4 estimates from the GOSAT data (Parker et al., 2011), which uses XCO_2 from the Carbontracker model (Peters et al., 2007), with a preliminary estimate of XCO_2 that is derived by assimilating GOSAT XCO_2 estimates into the land/ocean/atmosphere global carbon models developed for the NASA Carbon Monitoring System or CMS (e.g., Liu et al., 2014). A comparison between these revised lower tropospheric estimates and the GEOS-Chem lower tropospheric values is shown as the green line in Fig. 9 and shows substantially larger

differences between the comparison shown by the red line, resulting in up to 50 ppb difference in the lower tropospheric methane derived using these preliminary XCO_2 estimates (difference between green and red line). The comparisons shown in Fig. 9 gives more confidence in the lower tropospheric methane estimates based on the carbontracker XCO_2; however, this comparison highlights the importance of accurate XCO_2 fields for quantifying both XCH_4 and lower tropospheric CH_4 concentrations.

4 Conclusions

This study shows the potential for estimating lower-tropospheric methane concentrations using a combination of thermal IR and reflected sunlight measurements. Here we report monthly averaged lower tropospheric methane concentrations (lowermost 250 hPa of the atmosphere) for July 2009 on a $4^\circ \times 5^\circ$ grid. The spatiotemporal resolution is driven by the sampling of the TES and GOSAT instruments. The smoothing error is approximately 10 ppb or less and the calculated precision at this spatiotemporal resolution varies between approximately 10 and 30 ppb. We find that the lower tropospheric measurements from GOSAT/TES are biased low by approximately 65 ± 6 ppb by comparing these data to those from the GEOS-Chem model and GEOS-Chem to surface measurements. However, additional comparisons with ground and aircraft measurements for different seasons are needed to ensure these estimates of the bias and its errors are robust.

Both the GEOS-Chem model and these new lower tropospheric methane estimates broadly show the same inter-hemispheric gradient and enhanced concentrations over regions with large important methane fluxes. However, model/data differences are larger than the calculated errors (both precision and accuracy) for northern Canada, Southeast Asia, the tropical wetlands, and a region between the Black and Caspian seas; these regions should be the subject of a future study.

The current approach can resolve lower-tropospheric concentrations at monthly time scales on a 4×5 grid. However, many of the key processes controlling wetland fluxes such as rainfall, flooding, or the freeze and thaw of snow and ice occur at time-scales of much less than a month and at finer spatial scales (e.g., Bloom et al., 2012; Melton et al., 2013; Kort et al., 2014, and many references therein). Consequently it is desirable for an instrument designed to characterize the processes controlling methane to jointly measure the thermal and near-IR radiances for CH_4 retrievals at much finer spatial and temporal resolution. A Geo-orbiting satellite with a combined thermal and near-IR capability would greatly improve the spatiotemporal sampling and uncertainty of lower-tropospheric estimates. Combining IR-based CH_4 measurements from the Atmospheric Infrared Sounder (AIRS), Infrared Atmospheric Sounding Interferometer (IASI), or the Cross-track Infrared Sounder (CrIS) with total column CH_4 measurements from GOSAT or the next-generation TropOMI instruments, along with better estimates of total column CO_2 from OCO-2 will also greatly enhance our ability to resolve near-surface methane concentrations, improving sensitivity to estimate methane fluxes, especially at higher latitudes.

Appendix A: Description of GEOS-Chem model

We use the v9-01-02 GEOS-Chem methane simulation (http://acmg.seas.harvard.edu/geos/index.html; Pickett-Heaps et al., 2011; Wecht et al., 2012, 2014; Turner et al., 2015) driven by Goddard Earth Observing System (GEOS-5) assimilated meteorological data from the NASA Global Modeling and Assimilation Office (GMAO). The GEOS-5 data have a native horizontal resolution of $\frac{1}{2}^\circ \times \frac{2}{3}^\circ$ with 72 terrain-following pressure levels and 6 h temporal resolution (3 h for surface variables and mixing depths). Here we use the global methane simulation at $4^\circ \times 5^\circ$ resolution. The main methane sink is tropospheric oxidation by the OH radical. We use a three-dimensional archive of monthly average OH concentrations from Park et al. (2004), resulting in an atmospheric lifetime of 8.9 years.

Emissions for the GEOS-Chem methane simulation are from the EDGARv4.2 anthropogenic methane inventory (European Commission, 2011), the wetland model from Kaplan (2002) as implemented by Pickett-Heaps et al. (2011), the GFED3 biomass burning inventory (van der Werf et al., 2010), a termite inventory and soil absorption from Fung et al. (1991), and a biofuel inventory from Yevich and Logan (2003). Wetland emissions vary with local temperature, inundation, and snow cover. Open fire emissions are specified with 8 h temporal resolution. Other emissions are assumed aseasonal. Turner et al. (2015) lists global emissions for 2009–2011 and their shows spatial distributions.

Appendix B: Summary of TES and GOSAT retrieval uncertainties

We use Version 6 of the TES CH_4 data from the "Lite" product files (http://tes.jpl.nasa.gov/data/). A full description of the errors for TES retrievals is provided in Worden et al. (2004) with the basic error analysis theory described in Bowman et al. (2006) and Worden et al. (2012). These errors include the effects of noise as well as radiative interferences from trace gases that absorb and emit in the 8 micron methane band such as H_2O, ozone, and N_2O, as well as the effects of temperature and emissivity.

We use the XCH_4 retrievals discussed in Parker et al. (2011). A description of the errors for GOSAT CH_4 retrievals is discussed in Butz et al. (2010, 2011), Parker et al. (2011), and Schepers et al. (2012) and references therein and includes the effects of noise, aerosols, and surface albedo. Uncertainties for both the TES and GOSAT retrievals range from 8 to 20 ppb (or 1 % or less). All TES and GOSAT products include uncertainties, the a priori and averaging kernel matrices. In this paper we only derive the uncertainties that result from estimating lower tropospheric methane from combining TES and GOSAT methane retrievals.

Appendix C: Description of WDCGC data

Lower tropospheric CH_4 concentrations are compared against July 2009 CH_4 measurements from 25 Global Atmospheric Watch (GAW) sites. Measurements are obtained from World Data Centre for Greenhouse Gases (WDCGG, http://ds.data.jma.go.jp/gmd/wdcgg/) website source. Monthly surface CH_4 concentrations are based on stationary platform continuous and flask air sampling observations. Figure C1 shows the locations of the measurements used for the comparison. Data are selected if they corresponded to one of the 5° lon $\times 4^\circ$ lat estimates derived from the GOSAT/TES measurements, and therefore only land measurements are usable for this comparison.

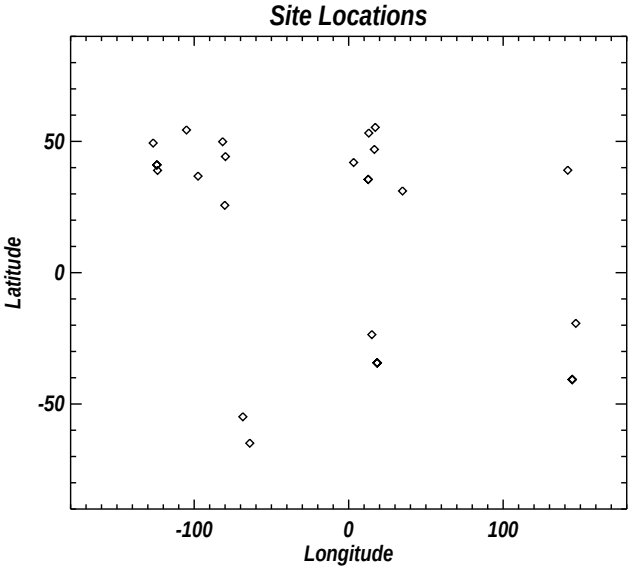

Figure C1. Coordinates of the surface data used in the comparison shown in Fig. 9.

Acknowledgements. Part of this research was carried out at the Jet Propulsion Laboratory, California Institute of Technology, under a contract with the National Aeronautics and Space Administration. A. J. Turner was supported by a Computational Science Graduate Fellowship (CSGF). This research was funded by NASA ROSES CSS proposal 13-CARBON13_2-0071 and the NASA Carbon Monitoring System. The GOSAT XCH_4 data were generated with funding from the UK National Centre for Earth Observation and the ESA GHG-CCI project with the GOSAT L1B data kindly provided by JAXA/NIES/MOE. Methane surface data were downloaded from the World Data Centre for Greenhouse Gases. We are very grateful to all the institutions and individuals who provide these surface data for researchers to use as these efforts are critical for carbon cycle science research; the following is hopefully an inclusive list institutions and individuals, based on email response, who provide data that we use in this research: (1) NOAA, Boulder CO/Ed Dlugokencky, Laboratory for Earth Observations and Analyses, (2) ENEA, Palermo, Italy/Salvatore Piacentino, the CSIRO Flask Network/Paul Krummel, (3) Atmospheric Environment Division, Global Environment and Marine Department Japan Meteorological Agency/Atsushi Takizawa, and (4) Canadian Greenhouse Gas Measurement Program, Environment Canada/Doug Worthy.

Edited by: W. R. Simpson

References

Alvarado, M. J., Payne, V. H., Cady-Pereira, K. E., Hegarty, J. D., Kulawik, S. S., Wecht, K. J., Worden, J. R., Pittman, J. V., and Wofsy, S. C.: Impacts of updated spectroscopy on thermal infrared retrievals of methane evaluated with HIPPO data, Atmos. Meas. Tech., 8, 965–985, doi:10.5194/amt-8-965-2015, 2015.

Bergamaschi, P., Houweling, S., Segers, A., Krol, M., Frankenberg, C., Scheepmaker, R. A., Dlugokencky, E., Wofsy, S. C., Kort, E. A., Sweeney, C., Schuck, T., Brenninkmeijer, C., Chen, H., Beck, V., and Gerbig, C.: Atmospheric CH_4 in the first decade of the 21st century: Inverse modeling analysis using SCIAMACHY satellite retrievals and NOAA surface measurements, J. Geophys. Res.-Atmos., 118, 7350–7369, doi:10.1002/jgrd.50480, 2013.

Bey, I., Jacob, D., Yantosca, R., Logan, J., Field, B., Fiore, A., Li, Q., Liu, H. Y., Mickley, L., and Schultz, M. G.: Global modeling of tropospheric chemistry with assimilated meteorology: Model description and evaluation, J. Geophys. Res.-Atmos., 106, 23073–23095, 2001.

Bloom, A. A., Palmer, P. I., Fraser, A., Reay, D. S., and Frankenberg, C.: Large-Scale Controls of Methanogenesis Inferred from Methane and Gravity Spaceborne Data, Science, 327, 322–325, doi:10.1126/science.1175176, 2010.

Bloom, A. A., Palmer, P. I., Fraser, A., and Reay, D. S.: Seasonal variability of tropical wetland CH_4 emissions: the role of the methanogen-available carbon pool, Biogeosciences, 9, 2821–2830, doi:10.5194/bg-9-2821-2012, 2012.

Bowman, K. W., Rodgers, C. D., Kulawik, S. S., Worden, J., Sarkissian, E., Osterman, G., Steck, T., Lou, M., Eldering, A. and Shephard, M.: Tropospheric emission spectrometer: Retrieval method and error analysis, IEEE T. Geosci. Remote Sens., 44, 1297–1307, 2006.

Butz, A., Hasekamp, O. P., Frankenberg, C., Vidot, J., and Aben, I.: CH_4 retrievals from space-based solar backscatter measurements: Performance evaluation against simulated aerosol and cirrus loaded scenes, J. Geophys. Res, 115, D24302, doi:10.1029/2010JD014514, 2010.

Butz, A., Guerlet, S., Hasekamp, O., Schepers, D., Galli, A., Aben, I., Frankenberg, C., Hartmann, J. M., Tran, H., Kuze, A., Keppel-Aleks, G., Toon, G., Wunch, D., Wennberg, P., Deutscher, N., Griffith, D., Macatangay, R., Messerschmidt, J., Notholt, J. and Warneke, T.: Toward accurate CO_2 and CH_4 observations from GOSAT, Geophys. Res. Lett., 38, L14812, doi:10.1029/2011GL047888, 2011.

Connor, B. J., Boesch, H., Toon, G., Sen, B., Miller, C., and Crisp, D.: Orbiting Carbon Observatory: Inverse method and prospective error analysis, J. Geophys. Res, 113, D05305, doi:10.1029/2006JD008336, 2008.

European Commission: Emission Database for Global Atmospheric Research (EDGAR), release version 4.2, Tech. rep., Joint Research Centre (JRC)/Netherlands Environmental Assessment Agency (PBL), available at: http://edgar.jrc.ec.europa.eu (last access: 1 December 2014), 2011.

Frankenberg, C., Meirink, J., Van Weele, M., Platt, U., and Wagner, T.: Assessing methane emissions from global space-borne observations, Science, 308, 1010–1014, doi:10.1126/science.1106644, 2005.

Frankenberg, C., Aben, I., Bergamaschi, P., Dlugokencky, E. J., van Hees, R., Houweling, S., van der Meer, P., Snel, R., and Tol, P.: Global column-averaged methane mixing ratios from 2003 to 2009 as derived from SCIAMACHY: Trends and variability, J. Geophys. Res, 116, D04302, doi:10.1029/2010JD014849, 2011.

Fung, I., John, J., Lerner, J., Matthews, E., Prather, M., Steele, L. P., and Fraser, P. J.: Three-dimensional model synthesis of the global methane cycle, J. Geophys. Res., 96, 13033, doi:10.1029/91jd01247, 1991.

Jiang, Z., Jones, D. B. A., Worden, H. M., Deeter, M. N., Henze, D. K., Worden, J., Bowman, K. W., Brenninkmeijer, C. A. M., and Schuck, T. J.: Impact of model errors in convective transport on CO source estimates inferred from MOPITT CO retrievals, J. Geophys. Res.-Atmos., 118, 2073–2083, doi:10.1002/jgrd.50216, 2013.

Jiang, Z., Jones, D. B. A., Worden, J., Worden, H. M., Henze, D. K., and Wang, Y. X.: Regional data assimilation of multispectral MOPITT observations of CO over North America, Atmos. Chem. Phys., 15, 6801–6814, doi:10.5194/acp-15-6801-2015, 2015.

Kaplan, J. O.: Wetlands at the Last Glacial Maximum: Distribution and methane emissions, Geophys. Res. Lett., 29-, 1079, doi:10.1029/2001GL013366, 2002.

Keppel-Aleks, G., Wennberg, P. O., and Schneider, T.: Sources of variations in total column carbon dioxide, Atmos. Chem. Phys., 11, 3581–3593, doi:10.5194/acp-11-3581-2011, 2011.

Keppel-Aleks, G., Wennberg, P. O., Washenfelder, R. A., Wunch, D., Schneider, T., Toon, G. C., Andres, R. J., Blavier, J.-F., Connor, B., Davis, K. J., Desai, A. R., Messerschmidt, J., Notholt, J., Roehl, C. M., Sherlock, V., Stephens, B. B., Vay, S. A., and Wofsy, S. C.: The imprint of surface fluxes and transport on variations in total column carbon dioxide, Biogeosciences, 9, 875–891, doi:10.5194/bg-9-875-2012, 2012.

Kort, E. A., Frankenberg, C., Costigan, K. R., Lindenmaier, R., Dubey, M. K., and Wunch, D.: Four corners: The largest US methane anomaly viewed from space, Geophys. Res. Lett., 10, 6898, doi:10.1002/2014GL061503, 2014.

Kuai, L., Worden, J., Kulawik, S., Bowman, K., Lee, M., Biraud, S. C., Abshire, J. B., Wofsy, S. C., Natraj, V., Frankenberg, C., Wunch, D., Connor, B., Miller, C., Roehl, C., Shia, R.-L., and Yung, Y.: Profiling tropospheric CO_2 using Aura TES and TCCON instruments, Atmos. Meas. Tech., 6, 63–79, doi:10.5194/amt-6-63-2013, 2013.

Liu, J., Bowman, K. W., Lee, M., Henze, D. K., Bousserez, N., Brix, H., Collatz, G. J., Menemenlis, D., Ott, L. E., Pawson, S., Jones, D. B. A., and Nassar, R.: Carbon monitoring system flux estimation and attribution: impact of ACOS-GOSAT XCO_2 sampling on the inference of terrestrial biospheric sources and sinks, Tellus B, 66, 22486, doi:10.3402/tellusb.v66.22486, 2014.

Melton, J. R., Wania, R., Hodson, E. L., Poulter, B., Ringeval, B., Spahni, R., Bohn, T., Avis, C. A., Beerling, D. J., Chen, G., Eliseev, A. V., Denisov, S. N., Hopcroft, P. O., Lettenmaier, D. P., Riley, W. J., Singarayer, J. S., Subin, Z. M., Tian, H., Zürcher, S., Brovkin, V., van Bodegom, P. M., Kleinen, T., Yu, Z. C., and Kaplan, J. O.: Present state of global wetland extent and wetland methane modelling: conclusions from a model intercomparison project (WETCHIMP), Biogeosciences, 10, 753–788, doi:10.5194/bg-10-753-2013, 2013.

O'Dell, C. W., Connor, B., Bösch, H., O'Brien, D., Frankenberg, C., Castano, R., Christi, M., Eldering, D., Fisher, B., Gunson, M., McDuffie, J., Miller, C. E., Natraj, V., Oyafuso, F., Polonsky, I., Smyth, M., Taylor, T., Toon, G. C., Wennberg, P. O., and Wunch, D.: The ACOS CO2 retrieval algorithm – Part 1: Description and validation against synthetic observations, Atmos. Meas. Tech., 5, 99–121, doi:10.5194/amt-5-99-2012, 2012.

Ott, L. E., Pawson, S., Collatz, G. J., Gregg, W. W., Menemenlis, D., Brix, H., Rousseaux, C. S., Bowman, K. W., Liu, J. and Eldering, A.: Assessing the magnitude of CO_2 flux uncertainty in atmospheric CO_2 records using products from NASA's Carbon Monitoring Flux Pilot Project, J. Geophys. Res.-Atmos., 120, 734, doi:10.1002/2014JD022411, 2015.

Park, R. J., Jacob, D. J., Field, B. D., Yantosca, R. M., and Chin, M.: Natural and transboundary pollution influences on sulfate-nitrate-ammonium aerosols in the United States: implications for policy, J. Geophys. Res.Atmos., 109, D15204, doi:10.1029/2003jd004473, 2004.

Parker, R., Boesch, H., Cogan, A., Fraser, A., Feng, L., Palmer, P. I., Messerschmidt, J., Deutscher, N., Griffith, D. W. T., Notholt, J., Wennberg, P. O., and Wunch, D.: Methane observations from the Greenhouse Gases Observing SATellite: Comparison to ground-based TCCON data and model calculations, Geophys. Res. Lett, 38, L15807, doi:10.1029/2011GL047871, 2011.

Peters, W., Jacobson, A. R., Sweeney, C., Andrews, A. E., Conway, T. J., Masarie, K., Miller, J. B., Bruhwiler, L. M., Pétron, G., and Hirsch, A. I.: An atmospheric perspective on North American carbon dioxide exchange: CarbonTracker, Proc. Natl. Acad. Sci. USA, 104, 18925–18930, 2007.

Pickett-Heaps, C. A., Jacob, D. J., Wecht, K. J., Kort, E. A., Wofsy, S. C., Diskin, G. S., Worthy, D. E. J., Kaplan, J. O., Bey, I., and Drevet, J.: Magnitude and seasonality of wetland methane emissions from the Hudson Bay Lowlands (Canada), Atmos. Chem. Phys., 11, 3773–3779, doi:10.5194/acp-11-3773-2011, 2011.

Rodgers, C. D.: Inverse Methods for Atmospheric Sounding: Theory and Practice, World Scientific Publishing Co., Singapore, 2000.

Rodgers, C. D. and Connor, B. J.: Intercomparison of remote sounding instruments, J. Geophys. Res.-Atmos., 108, 4116, doi:10.1029/2002JD002299, 2003.

Schepers, D., Guerlet, S., Butz, A., Landgraf, J., Frankenberg, C., Hasekamp, O., Blavier, J. F., Deutscher, N. M., Griffith, D. W. T., Hase, F., Kyro, E., Morino, I., Sherlock, V., Sussmann, R., and Aben, I.: Methane retrievals from Greenhouse Gases Observing Satellite (GOSAT) shortwave infrared measurements: Performance comparison of proxy and physics retrieval algorithms, J. Geophys. Res, 117, D10307, doi:10.1029/2012JD017549, 2012.

Stephens, B. B., Gurney, K. R., Tans, P. P., Sweeney, C., Peters, W., Bruhwiler, L., Ciais, P., Ramonet, M., Bousquet, P., Nakazawa, T., Aoki, S., Machida, T., Inoue, G., Vinnichenko, N., Lloyd, J., Jordan, A., Heimann, M., Shibistova, O., Langenfelds, R. L., Steele, L. P., Francey, R. J., and Denning, A. S.: Weak northern and strong tropical land carbon uptake from vertical profiles of atmospheric CO_2, Science, 316, 1732–1735, doi:10.1126/science.1137004, 2007.

Turner, A. J., Jacob, D. J., Wecht, K. J., Maasakkers, J. D., Lundgren, E., Andrews, A. E., Biraud, S. C., Boesch, H., Bowman, K. W., Deutscher, N. M., Dubey, M. K., Griffith, D. W. T., Hase, F., Kuze, A., Notholt, J., Ohyama, H., Parker, R., Payne, V. H., Sussmann, R., Sweeney, C., Velazco, V. A., Warneke, T., Wennberg, P. O., and Wunch, D.: Estimating global and North American methane emissions with high spatial resolution using GOSAT satellite data, Atmos. Chem. Phys., 15, 7049–7069, doi:10.5194/acp-15-7049-2015, 2015.

van der Werf, G. R., Randerson, J. T., Giglio, L., Collatz, G. J., Mu, M., Kasibhatla, P. S., Morton, D. C., DeFries, R. S., Jin, Y., and van Leeuwen, T. T.: Global fire emissions and the contribution of deforestation, savanna, forest, agricultural, and peat fires (1997–2009), Atmos. Chem. Phys., 10, 11707–11735, doi:10.5194/acp-10-11707-2010, 2010.

Wecht, K. J., Jacob, D. J., Wofsy, S. C., Kort, E. A., Worden, J. R., Kulawik, S. S., Henze, D. K., Kopacz, M., and Payne, V. H.: Validation of TES methane with HIPPO aircraft observations: implications for inverse modeling of methane sources, Atmos. Chem. Phys., 12, 1823–1832, doi:10.5194/acp-12-1823-2012, 2012.

Wecht, K. J., Jacob, D. J., Sulprizio, M. P., Santoni, G. W., Wofsy, S. C., Parker, R., Bösch, H., and Worden, J.: Spatially resolving methane emissions in California: constraints from the CalNex aircraft campaign and from present (GOSAT, TES) and future (TROPOMI, geostationary) satellite observations, Atmos. Chem. Phys., 14, 8173–8184, doi:10.5194/acp-14-8173-2014, 2014.

Worden, H. M., Deeter, M. N., Edwards, D. P., Gille, J. C., Drummond, J. R., and Nedelec, P.: Observations of near-surface carbon monoxide from space using MOPITT multispectral retrievals, J. Geophys. Res., 115, D18314, doi:10.1029/2010JD014242, 2010.

Worden, J., Kulawik, S., Shepard, M., Clough, S., Worden, H., Bowman, K., and Goldman, A.: Predicted errors of tropospheric emission spectrometer nadir retrievals from spectral window selection, J. Geophys. Res., 109, D09308, doi:10.1029/2004JD004522, 2004.

Worden, J., Liu, X., Bowman, K., Chance, K., Beer, R., Eldering, A., Gunson, M., and Worden, H.: Improved tropospheric ozone

profile retrievals using OMI and TES radiances, Geophys. Res. Lett., 34, L01809, doi:10.1029/2006GL027806, 2007.

Worden, J., Kulawik, S., Frankenberg, C., Payne, V., Bowman, K., Cady-Peirara, K., Wecht, K., Lee, J.-E., and Noone, D.: Profiles of CH_4, HDO, H_2O, and N_2O with improved lower tropospheric vertical resolution from Aura TES radiances, Atmos. Meas. Tech., 5, 397–411, doi:10.5194/amt-5-397-2012, 2012.

Worden, J., Jiang, Z., Jones, D. B. A., Alvarado, M., Bowman, K., Frankenberg, C., Kort, E. A., Kulawik, S. S., Lee, M., Liu, J., Payne, V., Wecht, K., and Worden, H.: El Nino, the 2006 Indonesian Peat Fires, and the distribution of atmospheric methane, Geophys. Res. Lett, 40, 1, doi:10.1002/grl.50937, 2013.

Xiong, X., Barnet, C., Maddy, E., Wofsy, S. C., Chen, L., Karion, A., and Sweeney, C.: Detection of methane depletion associated with stratospheric intrusion by atmospheric infrared sounder (AIRS), Geophys. Res. Lett., 40, 2455–2459, doi:10.1002/grl.50476, 2013.

Yevich, R. and Logan, J. A.: An assessment of biofuel use and burning of agricultural waste in the developing world, Global Biogeochem. Cy., 17, 1095, doi:10.1029/2002gb001952, 2003.